A Bio-Inspired Robot With Undulatory Fins and Its Control Methods

Shuo Wang, Yu Wang, Qingping Wei, Min Tan, and Junzhi Yu, *Senior Member, IEEE*

***Abstract*—This paper proposes a bio-inspired robot with undulatory fins and summarizes its control methods. First, three basic motions, forward/backward swimming, diving/rising motion, and turning, are implemented and evaluated by experiments. Next, a hybrid control that combines active disturbance rejection control with a fuzzy strategy is presented to achieve closed-loop depth and course control according to the evaluation of the three basic motions. Finally, waypoint tracking with a line-of-sight guidance system based on a finite-state machine for this bio-inspired robot is presented. The results of swimming experiments are provided to illustrate the validity of the proposed methods.**

***Index Terms*—Bio-inspired robot, course control, depth control, waypoint tracking.**

I. Introduction

NATURAL selection can evolve innovative designs with strong adaptability, and this is also true for fish species. Fish swimming modes with thrust-generating fish fins can be classified into two types: body and/or caudal fin (BCF) and median and/or paired fin (MPF) [1]. The benefits of bio-inspired propulsion can inspire the design of autonomous underwater vehicles.

BCF swimming mode can be seen in 85% of fish species, which produce a large thrust by oscillating their bodies and caudal fins [2]. Thus, fish can move with high efficiency and great maneuverability at high speeds. Research on bio-inspired robotic prototypes that can use BCF locomotion can be found in [3]–[6]. MPF swimming mode is commonly seen in stingrays or knifefish. This mode achieves motion with good propulsive efficiency and high stability at low speeds. These fish have a large flat body that is stable during locomotion. This is a promising design for robotic fish and underwater vehicles, because instruments or sensors can be installed inside the body [7]. Using the research on the wave-like propulsion mechanism and hydrodynamics analysis, many bio-inspired robotic prototypes have been developed to verify the MPF swimming mode mechanisms and study their bionical motion. Wang *et al.* developed a robotic prototype with disc-like pectoral fins and gave its kinematic model [8]. Allotta *et al.* developed a U-CAT prototype with four oscillating flippers to implement high maneuver abilities [9]. Analogously, the Aqua prototype is developed, which uses six oscillating flippers to achieve underwater motion [10], [11].

Biologically inspired robotic prototypes with a single long fin have been developed to perform the undulating locomotion and test the propulsion mechanism. Curet *et al.* developed a bio-inspired robotic knifefish that mimics the motion of a black ghost knifefish. An optimal operational region in the fin's kinematic parameter space was found [12]. Liu *et al.* developed a mechanical undulating fin, and gave its hydrodynamic model [13]. Low *et al.* developed a robotic prototype inspired by the black ghost knifefish. One single mechanical fin with a free baseline was used for propulsion [14], and an online search of optimal parameter sets for the central pattern generator (CPG) model was proposed to improve the performance of bio-inspired undulatory locomotion [15]. Zhang *et al*. designed a bioinspired underwater propulsor and studied controllable fin parameters [16]. Additionally, several bio-inspired robots with two symmetrical undulating fins have also been developed. Zhou and Low devised a bio-inspired underwater vehicle (BUV) with two flapping pectoral fins, which can achieve forward/backward swimming and turning maneuvers in two-dimensional (2-D) space by applications of CPGs [7]. Moreover, Wang *et al.* developed a BUV with two flapping pectoral fins [17] and Hu *et al.* proposed a learning control approach to implement effective phase tracking for this BUV [18]. Rahman *et al.* developed a bio-inspired robot with two undulating side fins and investigated the braking performance of this robot [19].

In the above references, the wave-like propulsion mechanism is mainly considered and discussed. This paper mainly focuses on the closed-loop control methods for the robot with undulatory fins. We developed a bio-inspired robot with undulatory fins called "RobCutt-I." Motivated by the need to promote the applications of the robot with two flapping pectoral fins, the main aim of this paper is to present and summarize control methods employed in "RobCutt-I," which include depth/course

Manuscript received October 30, 2015; revised April 25, 2016, July 16, 2016, and September 13, 2016; accepted October 19, 2016. Date of publication October 31, 2016; date of current version February 14, 2017. Recommended by Technical Editor S. Park. This work was supported in part by the National Natural Science Foundation of China under Grants 51175496, 61233014, and 61333016, and in part by the Foundation for Innovative Research Groups of the National Natural Science Foundation of China under Grant 61421004, and in part by the Beijing Natural Science Foundation under Grant 3141002. *(Corresponding authors: Yu Wang and Qingping Wei.)*

The authors are with the State Key Laboratory of Management and Control for Complex Systems, Institute of Automation, Chinese Academy of Sciences, Beijing 100190, China (e-mail: shuo.wang@ia.ac.cn; yu.wang@ia.ac.cn; weiqingping@126.com; min.tan@ia.ac.cn; junzhi.yu@ia.ac.cn).

Color versions of one or more of the figures in this paper are available online at http://ieeexplore.ieee.org.

Digital Object Identifier 10.1109/TMECH.2016.2622761

control and waypoint tracking. Thus, readers can be guided through a process of research on a bio-inspired robot with undulatory fins including development and control methods. This paper offers the following control methods for this robotic prototype.

1) Three basic motions, including forward/backward swimming, diving/rising, and turning are achieved using the wave-like propulsion mechanism. The relationship between locomotion speed and the kinematic parameters of the propagating waveform for "RobCutt-I" has been studied and evaluated by experiments.
2) Hybrid control that combines active disturbance rejection control (ADRC) with a fuzzy strategy is proposed to achieve closed-loop depth and course control based on the evaluation of the three basic motions. The ADRC controller outputs the force or torque for corresponding depth or course control, and the fuzzy method builds the relationship between the force or torque and the parameters of the propagating wave.
3) Waypoint tracking is presented for the robot with undulatory fins. This tracking consists of a line-of-sight (LOS) guidance system, three ADRC subcontrollers, and a fuzzy method for parameter mapping. The LOS guidance system based on finite-state machines (FSMs), is designed to help "RobCutt-I" track the waypoints in good order. Three ADRC subcontrollers each provide the feedback law for the torques or forces required to track the desired heave speed, depth, and course. The fuzzy method provides the relationship between the force or torque and the parameters of the propagating wave.

II. "RobCutt-I" Overview

Manta rays achieve 3-D swimming locomotion generated by two pectoral fins. The mechanical structure of "RobCutt-I" was inspired by the morphology and locomotion modes of manta rays. This mechanism is based on our previous prototype [20], [21]. For simplicity, the following assumptions are made: 1) the pectoral fin is elastic and its thickness is ignored; 2) the baseline of the designed pectoral fin is simplified to a straight line. The resulting mechanism of "RobCutt-I" is schematically shown in Fig. 1. This robot is composed of a main body and two elastic long fins respectively installed on both sides of the main body. In the main body, all electronic equipment, power supply, control circuit, servo motors, and a depth sensor are placed. Sanyo's LiPo batteries are selected as power supply; The control circuit consists of PC104 controller and FPGA; BORCHE's CDS5516 servo motors have been used to control fin rays; CTG505 depth sensor which Kunshan Bridging Sensor Control Technology Company develops is used to measure water depth. Both mechanical long fins consist of six fin rays mainly because a complete sine wave can be achieved by a long fin. Fin rays are connected to one another by a flexible membrane made of thin rubber. Each fin ray is driven by a corresponding servo motor. Fig. 1(b) shows the actuating system of each fin ray. The oscillating motion of the fin ray is transformed from the rotation of its corresponding servo motor through a gear transmission system. The gear transmission system is composed of two bevel gears that are coupled orthogonally. The transmission ratio between the two gears is 1:1. The corresponding technical specifications of the developed robot with undulatory fins are further detailed in Table I, where wave number represents the number of a complete sine wave which the long fin can generate. The center of gravity is at the bottom of the center of buoyancy, and the relative height between the centers of gravity and buoyancy is sufficiently large to guarantee high stability. Thus, the design of the robot with undulatory fins is complete.

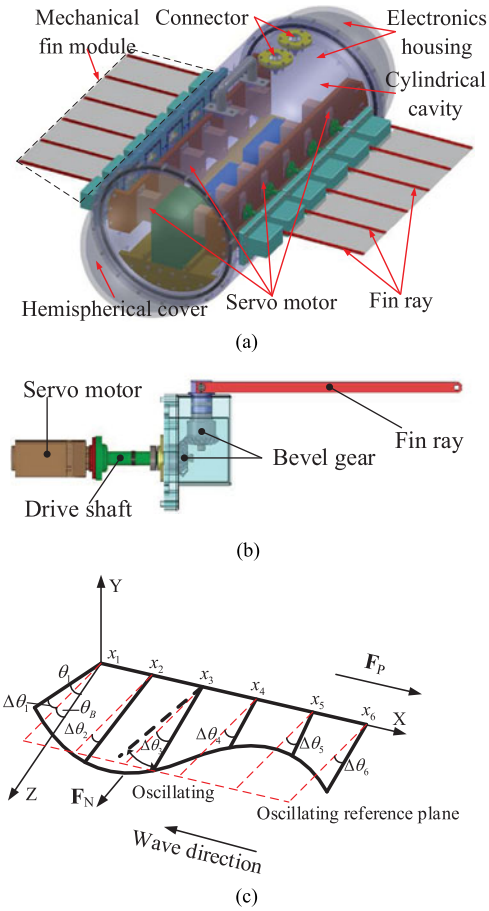

Fig. 1. Mechanical design of "RobCutt-I". (a) Design concept. (b) Actuating system for each fin ray. (c) Vector analysis of the undulating fin.

TABLE I
Technical Specification of the Bio-Inspired Robotic Prototype

Items	Characteristics
Total mass	27.2 kg
Body length	778 mm
Body diameter	236 mm
Wave frequency	0–4 Hz
Wave amplitude	10°–40°
Wave number	0–1
Fin length	360 mm
Fin width	130 mm
Space of fin rays	67 mm
Deflection angle	−50° to 50°
Power supply	Lithium-Polymer

An indoor swimming pool in the Institute of Automation Chinese Academy of Sciences (CASIA) is used for the BUV's swimming activities. Its dimensions (L × W × H) are

$5 \times 4 \times 1.1$ m. A global real-time vision system installed on the ceiling is connected to a host PC, and a water pressure sensor is mounted on "RobCutt-I," which obtains the robot's depth information. Therefore, the pose of "RobCutt-I" can be obtained by sensor fusion of the global vision and water pressure sensor. We next introduce the achievements of control methods including 3-D motion control, closed-loop depth, and course control, and waypoint tracking.

III. Basic Motion Control

A. Model Analysis of the Undulating Fin

The steady swimming locomotion of Manta rays is achieved by two pectoral fins. The undulating mode of pectoral fins is a periodic rhythmic motion, which can produce periodic waveforms. The waveforms are generated by modulating the lead-lag relationship of the oscillating motion between two adjacent fin rays, which are closely related to essential parameters including the undulation amplitude, the undulation wavelength, the undulation frequency, and the phase difference between fin-ray [18]. The swimming direction (forwards or backwards) is determined by the direction of the propagating waves. The vector analysis of the undulating fin is illustrated in Fig. 1(c). The plane marked by red and dotted lines in Fig. 1(c) is the oscillating reference plane around which the oscillation occurs, and θ_B represents the deflection angle, which is the angle between the oscillating reference and horizontal planes. This angle can be adjusted by controlling the central line of every fin ray's oscillating motion. Therefore, the undulating motion of one side fin can be defined by

$$\theta_i = \Delta\theta_i + \theta_B = A\cos\left(2\pi f t \pm \frac{2\pi}{\lambda} x_i\right) + \theta_B \qquad (1)$$

where t represents time, $\theta_i (i = 1, 2, \ldots, 6)$ represents the deflection angle between the ith fin ray and horizontal plane at a certain time t, $\Delta\theta_i (i = 1, 2, \ldots, 6)$ represents the angle between the ith fin ray and the oscillating reference plane at a certain time t, A represents the wave amplitude, f represents the wave frequency, λ represents the wave length of the generated wave, x_i is the position of the ith fin ray along the base line, and $2\pi x_i/\lambda$ is the phase difference, which is equal to $\varphi \cdot (i-1)$. Here, φ denotes the phase difference between two adjacent fin rays and θ_B is the deflection angle of the long fin. Note that the propagating direction of the wave is determined by the "$\pm$" sign in (1). A plus sign indicates that the generated wave passes from the positive direction to the negative direction along the X-axis, while the minus sign generates a wave in the opposite direction along the long fin. The number of waves along the long fins relies on the oscillation phase difference between two adjacent fin rays and the number of fin rays. The thrust force generated by an undulating fin is a function of wave amplitude, wave frequency, and wave length [12]. Because the number of fin rays is constant in "RobCutt-I," wave amplitude and wave frequency are employed to achieve the motion of this robot. The thrust force generated by the undulating fin is a combination of F_N and F_P [see Fig. 1(c)]. Force F_N is defined as the force generated by the waveforms of the fin rays that is normal to the fin base and parallel to the oscillating central line. Force F_P is defined as the force generated by the waveforms of the fin rays that is parallel to fin base. The direction of F_P is opposite to the direction of the wave, which leads to forward or backward swimming. Force F_N can generate a diving or rising motion once the deflection angles of two side fins are equal and nonzero.

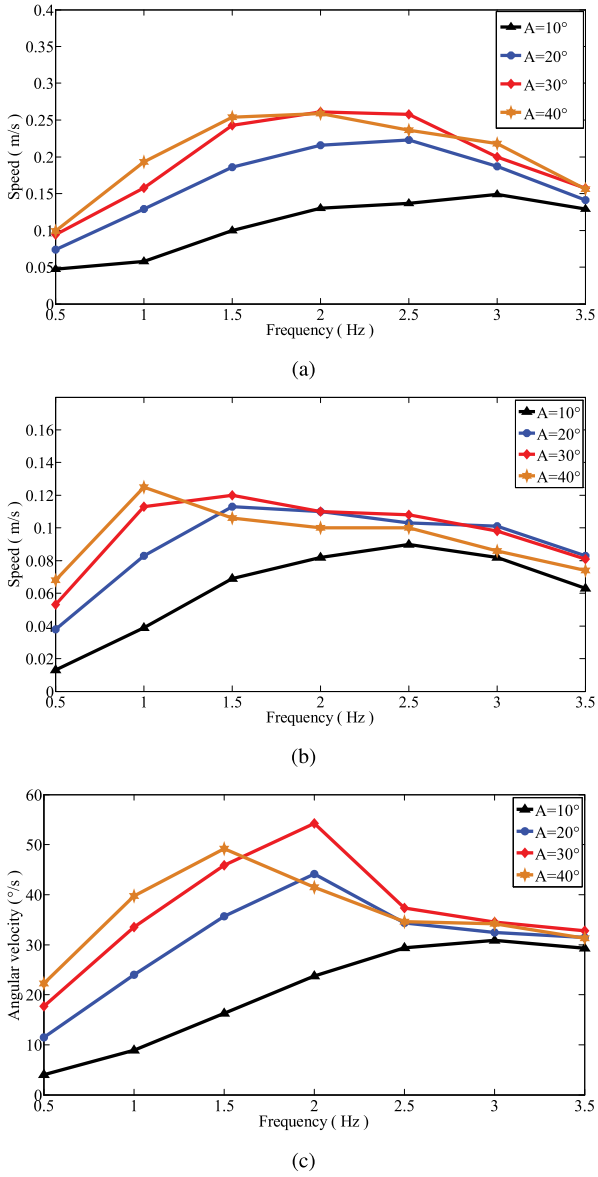

Fig. 2. Test and evaluation of the three basic motions. (a) Forward swimming speed evaluation by adjusting the wave frequency and/or amplitude with constant $\varphi = 57.6°$. (b) Diving speed evaluation by adjusting the wave frequency and/or amplitude with constant $\theta_B = -50°$. (c) Angular speed evaluation by adjusting the wave frequency and/or amplitude with constant $\varphi = 36°$.

B. Basic Motion Control and Evaluation

There are three basic motions: forward/backward swimming, diving/rising, and turning. Forward swimming can be achieved by $\theta_B = 0$ in (1). Moreover, the directions of the generated waves along the two fins are modulated consistently. Thus, the force F_P of each long fin has the same magnitude and direction, and the combination of the F_N forces cancels out. Fig. 2(a) shows the corresponding average swimming speed evaluation by adjusting the wave frequency and/or amplitude. In order to

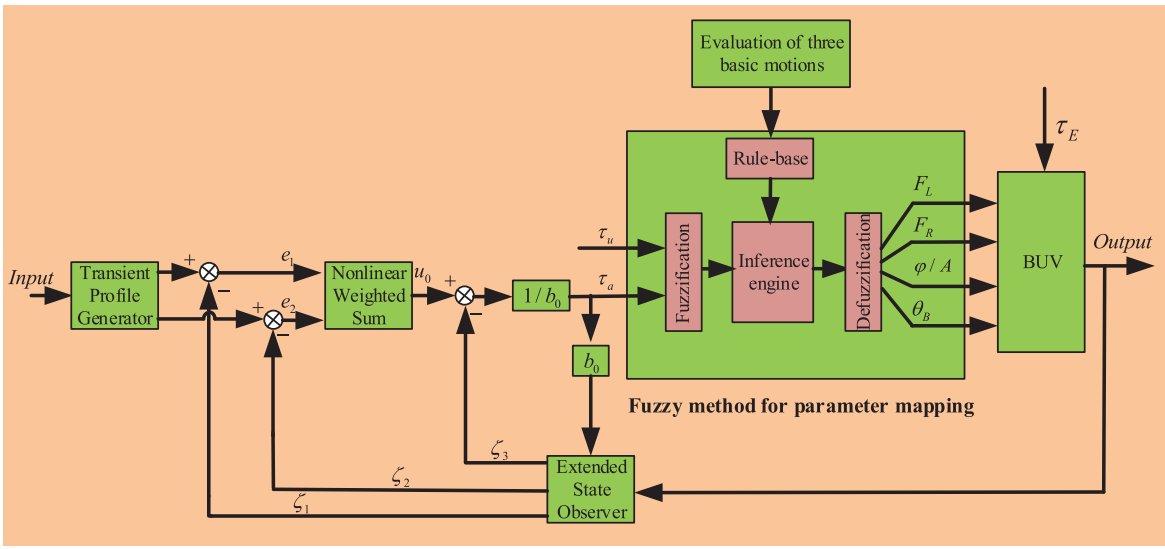

Fig. 3. Control block diagram of depth or course control.

swim backward, only the directions of the two waves need to be changed. Diving is achieved when $\theta_B < 0$ and $\varphi = 0$. Thus, the F_P generated by each fin becomes 0, and the combination of the F_N forces is vertical. Fig. 2(b) shows the corresponding average swimming speed evaluation by adjusting the wave frequency and/or amplitude. In order to realize a rising motion, it is only necessary for θ_B in (1) to be positive. A turning maneuver is achieved when the F_P generated by both side fins are different. The thrust difference depends on the wave amplitude and/or wave frequency and/or phase difference of both side fins. Another method to turn quickly can be implemented as well, where the two waves produced by the two side fins, respectively, propagate in different directions. Fig. 2(c) shows the corresponding average angular speed evaluation by adjusting the wave frequency and/or amplitude. Note that the fin actuation should be executed by changing from undulation with $\theta_B = 0$ to flapping with $\theta_B \neq 0$ to achieve the transition from surge to heave motion.

Note that the motion speed as a function of frequency forms a parabolic curve. This is because the amplitude decreases if the frequency is greater than a threshold value, which is related to the compliant nature of the actuators. An analogous curve which reflects the relationship between actuation and speed is also observed in similar underwater robots propelled by compliant actuators [22], [23]. From experiments on the three basic motions, we can analyze the relationship between thrust force or torque and the parameters of the propagating wave (here, force or torque is estimated and reflected according to the average speed), which can then provide the basis for closed-loop course/depth control and waypoint tracking.

IV. Closed-Loop Depth and Course Control

It is essential to achieve precise control of "RobCutt-I" (such as depth control and course control) for its applications. However, a robot with two flapping pectoral fins is a multivariable, nonlinear, and strong-coupling system, which is difficult to model accurately. We hence designed a hybrid control that combines ADRC with a fuzzy strategy to enable the robot with undulatory fins to achieve closed-loop depth and course control. The desired depth or course is used as the hybrid control input, and the actual depth or course is used as the hybrid control output. ADRC is used to estimate the general disturbances, including external disturbances, and model uncertainties in real time by use of an extended state observer (ESO). It then dynamically compensates for them in the control signal [24]. We employ an ADRC controller to output force or torque τ_a for the corresponding depth or course control, where τ_a denotes the heave force in depth control or yaw torque in course control. However, the relationship between force or torque and the parameters of the propagating wave, which is nonlinear, needs to be established. For engineering applications, a fuzzy parameter mapping method is proposed to build this relationship. The proposed control schedule for depth and course control is illustrated in Fig. 3. Here, τ_u represents the forward/backward force, which is obtained by ADRC controller for surge speed control. The parameters of the propagating wave consist of the left fin frequency, right fin frequency, phase difference, wave amplitude, and the deflection angle of the long fin, which are denoted by F_L, F_R, φ, A, and θ_B, respectively. Only four parameters of the propagating wave are needed to achieve depth control or course control. We choose φ as one of the four outputs in depth control, while A is chosen as one of the four outputs in course control (see Fig. 3). Because course control and depth control are similar, we only describe the proposed method for depth control.

A. ADRC Controller

The ADRC method, consisting of a transient profile generator, nonlinear weighted sum, and ESO was detailed by Han [24]. It does not rely on the accurate mathematical model of the controlled object, and inaccurate parameters can be tolerated. But the order of the system has to be known in advance. So, the general mathematical model which is simplified under certain conditions is given. The mathematical model of the vehicle with undulatory fins can be found in [13] and [24]. The math-

ematical model of "RobCutt-I" moving in 3-D space can then be developed using the inertial frame $O_E X_E Y_E Z_E$ and body-fixed frame $O_b X_b Y_b Z_b$. As depicted in Fig. 4, the gravity center of "RobCutt-I" is served as the origin of the body-fixed coordinate. "RobCutt-I" has good bilateral symmetry and fore-and-aft symmetry. In order to simplify the model, we give the following assumptions: The roll motion and pitch motion are ignored, because of not only the large height between the center of gravity and center of buoyancy but also the robot's relatively large contact area with water in the vertical direction. There is no coupling between diving motion and forwards swimming because that only small coupling between them exists. The surge and heave motions are decoupled from the sway and yaw motions. High frequency movement of "RobCutt-I" is ignored. The effect of nonlinear damping is neglected while linear damping is considered due to low speed of "RobCutt-I." Based on these assumptions, the mathematical model of "RobCutt-I" can then be simplified and described as follows [25]:

$$pp \begin{array}{l} \dot{\eta} = J(\psi)\nu \\ M\dot{\nu} = -C(\nu)\nu - D\nu + \tau + \tau_{\mathrm{E}} \end{array} \tag{2}$$

where

$$\begin{aligned} \eta &= [x\ y\ z\ \psi]^T, \nu = [u\ v\ w\ r]^T, \tau = [\tau_u\ 0\ \tau_w\ \tau_r]^T \\ \tau_E &= [\tau_{\mathrm{Eu}}\ \tau_{\mathrm{Ev}}\ \tau_{\mathrm{Ew}}\ \tau_{\mathrm{Er}}]^T \\ M &= \mathrm{diag}(m_{11}, m_{22}, m_{33}, m_{44}), \\ D &= \mathrm{diag}(d_{11}, d_{22}, d_{33}, d_{44}) \\ C &= \begin{bmatrix} 0 & 0 & 0 & -m_{22}v \\ 0 & 0 & 0 & m_{11}u \\ 0 & 0 & 0 & 0 \\ m_{22}v & -m_{11}u & 0 & 0 \end{bmatrix} \\ J &= \begin{bmatrix} \cos\psi & -\sin\psi & 0 & 0 \\ \sin\psi & \cos\psi & 0 & 0 \\ 0 & 0 & 1 & 0 \\ 0 & 0 & 0 & 1 \end{bmatrix} \end{aligned} \tag{3}$$

where x, y, z are the surge, sway, and heave displacement, respectively, with coordinates in inertial frame, ψ is the yaw angle of "RobCutt-I," u, v, w, r are surge, sway, heave, and yaw velocities with coordinates in body-fixed frame, control inputs τ_u and τ_w denote the surge and heave force, respectively, and τ_r denotes the yaw moment in body-fixed frame; $\tau_{\mathrm{Eu}}, \tau_{\mathrm{Ev}}, \tau_{\mathrm{Ew}}$ are the disturbance forces acting on surge, sway, heave, respectively, and τ_{Er} is the disturbance moment acting on yaw; $m_{11}, m_{22}, m_{33}, m_{44}$ denote the mass and added mass; $d_{11}, d_{22}, d_{33}, d_{44}$ denote the linear damping term and the effect of nonlinear damping is neglected. The estimation for parameters of mathematical model can be found in [25].

Using the mathematical model of "RobCutt-I," the dynamic equation of heave for depth control can be written as

$$\ddot{z} = f_w(\dot{z}, d_w) + b_w \tau_w \tag{4}$$

where $b_w = 1/m_{33}$, d_w represents the external disturbance, namely, $d_w = \tau_{\mathrm{Ew}}/m_{33}$, and $f_w(\dot{z}, d_w)$ represents the general disturbance including the external disturbance and internal

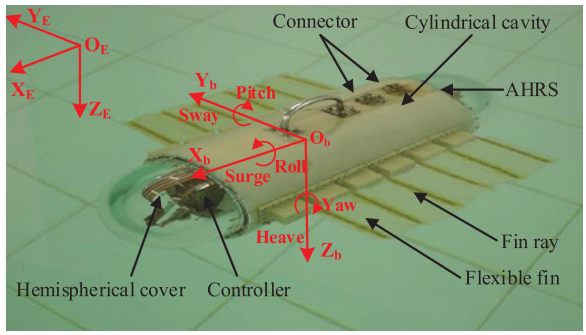

Fig. 4. The assigned frames in "RobCutt-I".

dynamics, which can be obtained as

$$f_w(\dot{z}, d_w) = -\frac{d_{33}}{m_{33}} w + \frac{1}{m_{33}} \tau_{\mathrm{Ew}}. \tag{5}$$

Therefore, the discrete time ADRC depth controller can be summarized as follows:

$$\begin{cases} z_1(k+1) = z_1(k) + h z_2(k) \\ z_2(k+1) = z_2(k) + h\,\mathrm{fhan}(z_1(k) - z_0(k), z_2(k), \delta, h_0) \\ e_w = z_1(k) - z(k) \\ \zeta_1(k+1) = \zeta_1(k) + h[\zeta_2(k) - l_{w1} e_w] \\ \zeta_2(k+1) = \zeta_2(k) + h[\zeta_3(k) - l_{w2} e_w + b_0 \tau_a] \\ \zeta_3(k+1) = \zeta_3(k) - h l_{w3} e_w) \\ e_1 = [z_1(k+1) - \zeta_1(k+1)] \\ e_2 = [z_2(k+1) - \zeta_2(k+1)] \\ u_0 = k_{\mathrm{pw}} e_1 + k_{\mathrm{dw}} e_2 \\ \tau_a = \frac{u_0 - \zeta_3(k+1)}{b_0} \end{cases} \tag{6}$$

where h denotes the control period of ADRC controller, k denotes the kth sample constant, e_1, e_2 denote state errors of ESO. z_0 denotes the desired depth as the input of the hybrid control, z_1 is the tracking signal of z_0, z_2 is the differential signal of z_1, z denotes the actual depth of "RobCutt-I," ζ_1 and ζ_2 are the estimated states of the dynamic heave equation, and ζ_3 is the extended state estimating the general disturbance. Furthermore, $l_{w1} = 3\omega_{\mathrm{ow}}, l_{w2} = 3{\omega_{\mathrm{ow}}}^2$, and $l_{w3} = {\omega_{\mathrm{ow}}}^3$ are ESO gains, w_{ow} is a tuning parameter that denotes the desired natural frequency of the closed-loop system, and τ_a is the output of ADRC controller, $\mathrm{fhan}(z_1(k) - z_0(k), z_2(k), \delta, h_0)$ is calculated as

$$\begin{cases} d = h_0 \delta^2 \\ a_0 = h_0 z_2 \\ y = z_1 + a + 0 \\ a_1 = \sqrt{d(d + 8|y|)} \\ a_2 = a_0 + \mathrm{sgn}(y)(a_1 - d)/2 \\ s_y = [\mathrm{sgn}(y + d) - \mathrm{sgn}(y - d)]/2 \\ a = (a_0 + y - a_2) s_y + a_2 \\ s_a = [\mathrm{sgn}(a + d) - \mathrm{sgn}(a - d)]/2 \\ \mathrm{fhan} = -\delta \left[\frac{a}{d} - \mathrm{sgn}(a)\right] s_a - \delta\,\mathrm{sgn}(a) \end{cases} \tag{7}$$

where $\mathrm{sgn}()$ denotes the symbolic function. In depth control, $\tau_a = \tau_w$, $b_0 = b_w$.

We next introduce the fuzzy method for determining the relationship between the heave force and the parameters of the propagating wave. The proposed fuzzy method consists of fuzzification, an inference engine, and defuzzification. Fuzzification transforms the crisp controlling quantity provided by the ADRC into fuzzy sets. A rule base is set up according to the evaluation of the three basic motions. The inference engine computes the fuzzy output based on the fuzzy input and rule base, where the commonly used and well known Mamdani's Max-Min method rule is adopted. Defuzzification retransforms the fuzzy outputs into crisp ones, where weighted average method is adopted. It can provide the rational parameters of the waves along the fins according to the evaluation of the three basic motions. The fuzzy method of depth control is given as follows. Fuzzy inference and defuzzification are omitted as the traditional methods are used.

B. Fuzzy Method for Parameter Mapping

1) Fuzzification: Fuzzification comprises the determination for variable sets, the selection of linguistic values, and selection of membership functions. According to the evaluation of the three basic motions, the universes of discourse is determined according to the experimental results of basic motion control: $\tau_u \in [-7, 7]$, $\tau_a \in [-5, 5]$, $F_L \in [-40, 40]$, $F_R \in [-40, 40]$, $\varphi \in [0, 40]$, $\theta_B \in [-170, 170]$, where the sign of the fin frequency represents the direction of the propagating wave. The sets for $\tau_u, \tau_a, F_L, F_R, \varphi$, and θ_B are represented as $T_u, T_a, U_{F_L}, U_{F_R}, U_\varphi$, and U_{θ_B}, respectively. The sets with seven linguistic values for τ_u, τ_a, F_L, and F_R are defined as $T_u = T_a = U_{F_L} = U_{F_R} = \{\mathrm{NB}, \mathrm{NM}, \mathrm{NS}, Z, \mathrm{PS}, \mathrm{PM}, \mathrm{PB}\}$. The set with four linguistic values for U_φ is defined as $U_\varphi = \{Z, \mathrm{PS}, \mathrm{PM}, \mathrm{PB}\}$; The set with five linguistic values for U_{θ_B} is defined as $U_{\theta_B} = \{\mathrm{NB}, \mathrm{NS}, Z, \mathrm{PS}, \mathrm{PB}\}$. Here NB, NM, NS, Z, PS, PM, and PB are the linguistic values "negative large," "negative median," "negative small," "zero," "positive small," "positive median," and "positive large," respectively. Standard triangular membership functions are utilized, as shown in Fig. 5.

2) Rule Base: The rule base is generated directly from the evaluation of three basic motions. Four key principles need to be taken into account when generating the rule base, as follows.

1) Heave force in depth control is closely related to the deflection angle of the long fin (denoted as θ_B). Heave force increases as the deflection angle increases, and vice versa.
2) When the forward force is small and heave force is large, the deflection angle of the long fin and wave frequency along the two fins should both increase, while the phase difference between the two adjacent fin rays should decrease.
3) When the forward force is large and heave force is small, the deflection angle of the long fin and wave frequency along the two fins should both decrease, while the phase difference between two adjacent fin rays should increase.

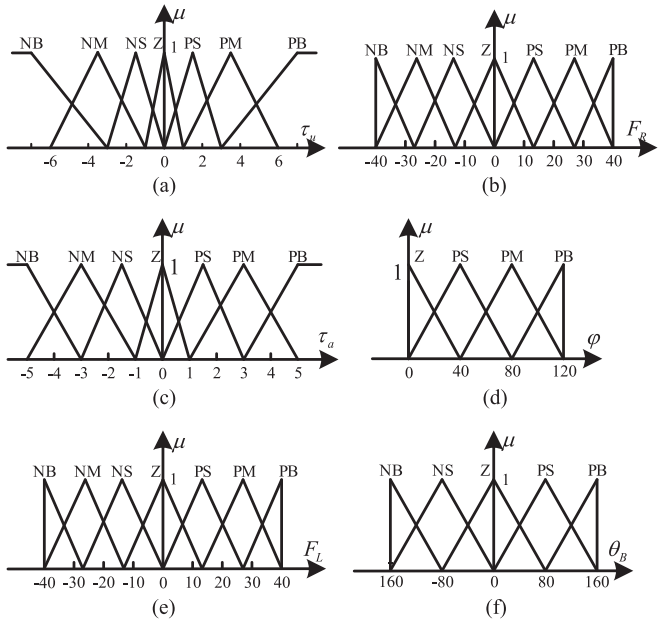

Fig. 5. Membership functions for: (a) τ_u, (b) F_R, (c) τ_a, (d) φ, (e) F_L, and (f) θ_B.

4) The priority of the depth control is higher than the priority of the surge control. Namely, when the forward force and heave force are both large, a large heave force is preferred.

The specific rule base is listed in Table II.

C. Experiment Results

In order to show the feasibility and effectiveness of the proposed method, the experimental results of depth and course control for "RobCutt-I" in an indoor water pool are presented, as illustrated in Fig. 6. Fig. 6(a) and (c) shows the images and data of the depth control experiment, respectively. The initial depth of "RobCutt-I" was 0.03 m and the desired depth was 0.5 m. From the data, we can see that "RobCutt-I" could arrive at the desired depth without over-adjustment and enter a steady state. Fig. 6(b) and (d) shows the images and data of the course control experiment, respectively. In the course control, the desired course was changed after "RobCutt-I" entered its current steady state during its motions. The desired courses were $10°, 100°, 200°$, and $280°$, successively.

V. Waypoint Tracking

A. Problem Statement and Solution Description

The waypoint tracking problem that we consider in this paper can be described as follows. Position $p_v(x_v, y_v, z_v)$ denotes the position of "RobCutt-I" in the world frame called $O_E X_E Y_E Z_E$, and ψ_v denotes the yaw angle of "RobCutt-I" in the $O_E X_E Y_E Z_E$ frame. Furthermore, $p_0(x_0, y_0, z_0)$ denotes the initial position of "RobCutt-I" in the world frame, and ψ_0 denotes the initial yaw angle of "RobCutt-I" in the $O_E X_E Y_E Z_E$ frame. The desired path is composed of a series of given 3-D waypoints in the world frame: $WP = \{p_1, p_2, \ldots, p_n\}$, $p_i = (x_i, y_i, z_i) \in \mathbb{R}^3, i = 1, 2, \ldots, n$. For each waypoint $p_i, i =$

TABLE II
RULE BASE

U_{F_L}, U_{F_R},		T_a						
U_φ, U_{θ_B}		NB	NM	NS	Z	PS	PM	PB
T_u	NB	NB,NB, PB,PB	NB,NB, PB,PB	NB,NB, PB,PS	NB,NB, PB,Z	NB,NB, PB,NS	NB,NB, PB,NB	NB,NB, PB,NB
	NM	NB,NB, PS,PB	NM,NM, PM,PB	NM,NM, PB,PS	NM,NM, PB,Z	NM,NM, PB,NS	NM,NM, PM,NB	NB,NB, PS,NB
	NS	NB,NB, Z,PB	NM,NM, Z,PB	NM,NM, PS,PS	NS,NS, PM,Z	NM,NM, PS,NS	NM,NM, Z,NB	NB,NB, Z,NB
	Z	NB,NB, Z,PB	NM,NM, Z,PB	NM,NM, Z,PS	Z,Z, Z,Z	PM,PM, Z,NS	PM,PM, Z,NB	PB,PB, Z,NB
	PS	PB,PB, Z,PB	PM,PM, Z,PB	PM,PM, PS,PS	PS,PS, PM,Z	PM,PM, PS,NS	PM,PM, Z,NB	PB,PB, Z,NB
	PM	PB,PB, PS,PB	PM,PM, PM,PB	PM,PM, PB,PS	PM,PM, PB,Z	PM,PM, PB,NS	PM,PM, PM,NB	PB,PB, PS,NB
	PB	PB,PB, PB,PB	PB,PB, PB,PB	PB,PB, PB,PS	PB,PB, PB,Z	PB,PB, PB,NS	PB,PB, PB,NB	PB,PB, PB,NB

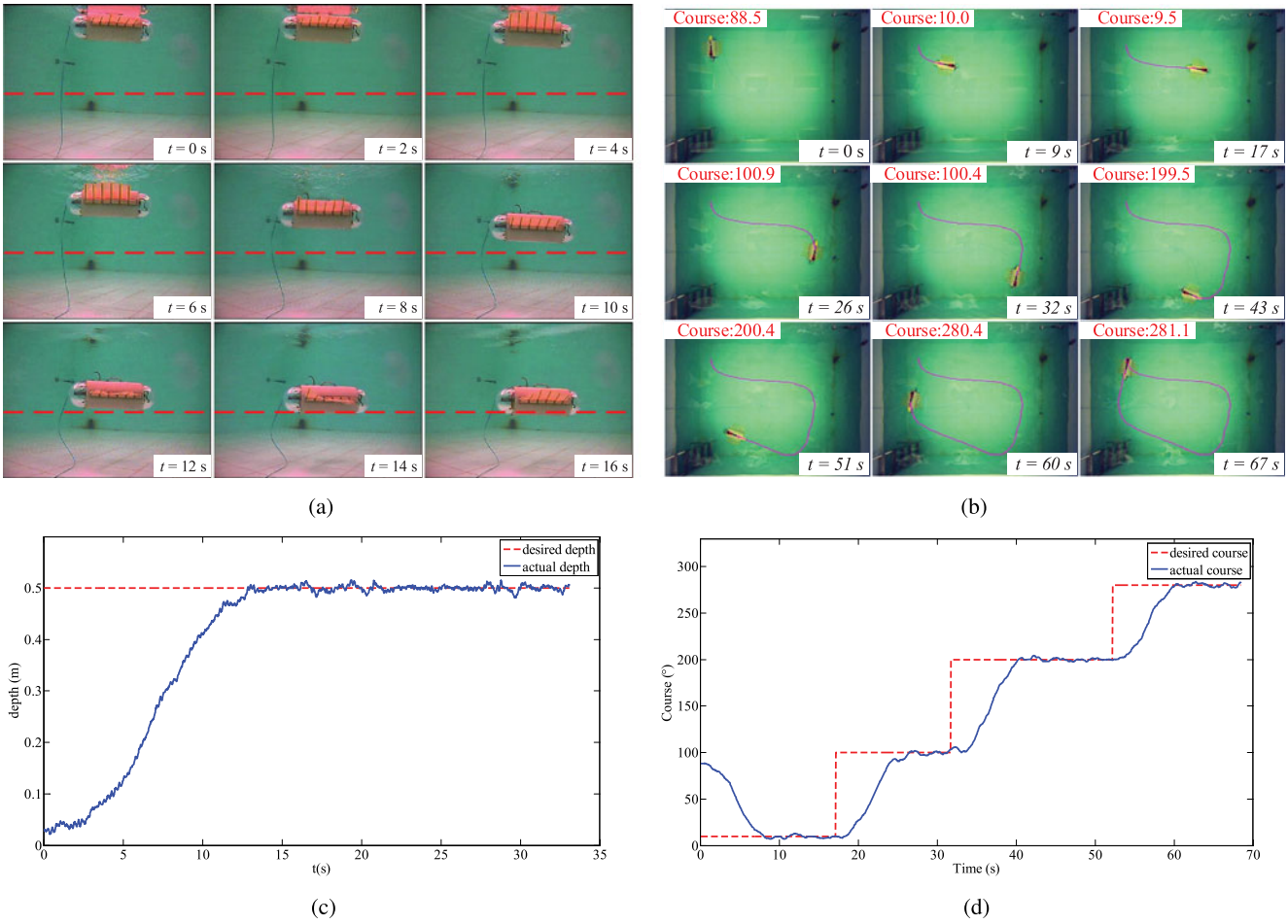

Fig. 6. Results of closed-loop depth and course control. (a) Images of the depth control experiment. (b) Images of the course control experiment. (c) Experimental results of depth control. (d) Experimental results of course control.

$1, 2, \ldots, n-1$, there is a closed ball $B_{\gamma_i}(p_i)$ with center p_i and $B_{\gamma_i}(p_i) = \{p \in \mathbb{R}^3 : \|p - p_i\| \leq \gamma_i, \gamma_i > 0\}$, where γ_i represents the radius of the ball.

The control objective is to force the robot's center of mass (x, y, z) to successively visit the neighborhoods of all waypoints except the last and to ultimately converge to the last waypoint p_n by designing a proper feedback control law for surge force τ_u, heave force τ_w, and yaw torque τ_r in the presence of unknown external environmental disturbances and model uncertainties.

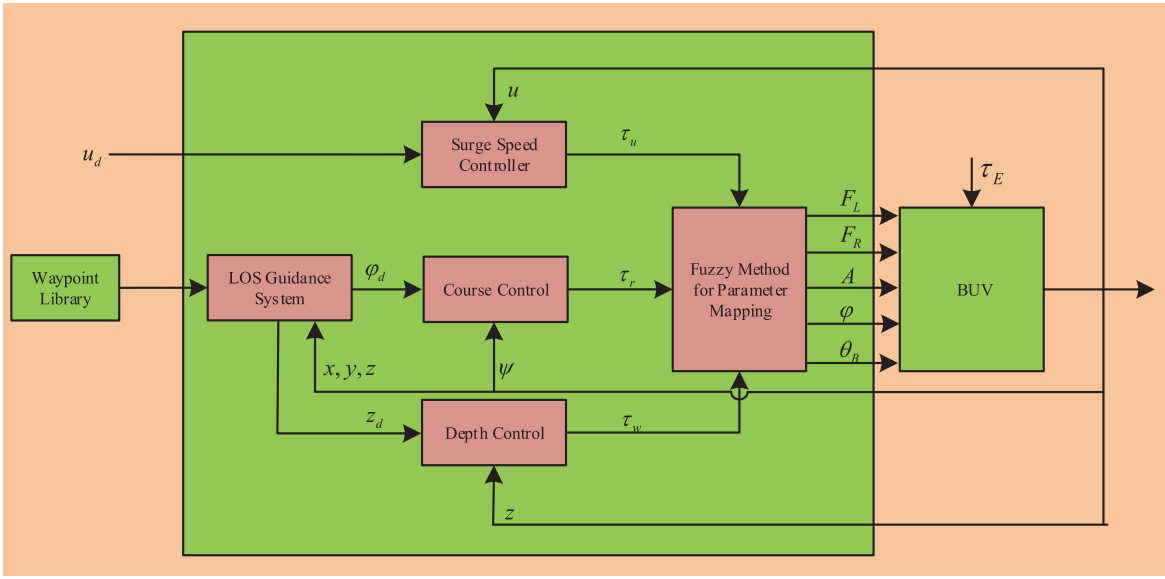

Fig. 7. Waypoint tracking control block diagram.

Note that for waypoint $p_i, i = 1, 2, \ldots, n-1$, it is more meaningful to minimize the cross-track error, defined as the distance from the robot's center of mass to the corresponding path segment defined by two adjacent waypoints, i.e., $L_{p_i p_{i+1}}, i = 1, 2, \ldots, n-1$, rather than to minimize the distance error between the robot's center of mass and the expected waypoint. Hence, the aim is to make "RobCutt-I" enter the neighborhoods of all the waypoints except for the final one. When "RobCutt-I" needs to reach the final waypoint, the distance error between the robot's center of mass and the last waypoint should be minimized. Hence "RobCutt-I" should be forced to eventually converge to the last waypoint, namely the radius of the last waypoint's neighborhood ball $B_{\gamma_n}(p_n)$ should be sufficiently small.

As depicted in Fig. 7, waypoint tracking for "RobCutt-I" is composed of a LOS guidance system, three ADRC subcontrollers, and a fuzzy method for parameter mapping. The LOS guidance system provides the expected yaw angle and expected depth based on the current state of "RobCutt-I" and the waypoint library. In the LOS guidance system, a FSM is employed to help "RobCutt-I" to track the waypoints in order. Three ADRC subcontrollers provide the feedback law for torques or forces to track the desired heave speed, course, and depth, respectively. A fuzzy parameter mapping method provides the relationship between the force or torque and the parameters of the propagating wave. Because the ADRC subcontroller and fuzzy method are similar to the ones for depth and course control, they are omitted here. We next describe the FSM-based LOS guidance system.

B. LOS Guidance System

The LOS guidance system plans "RobCutt-I" motion and is the core component of waypoint tracking. In the LOS guidance system, the FSM is designed to provide the desired course and depth in the next state according to the current state of

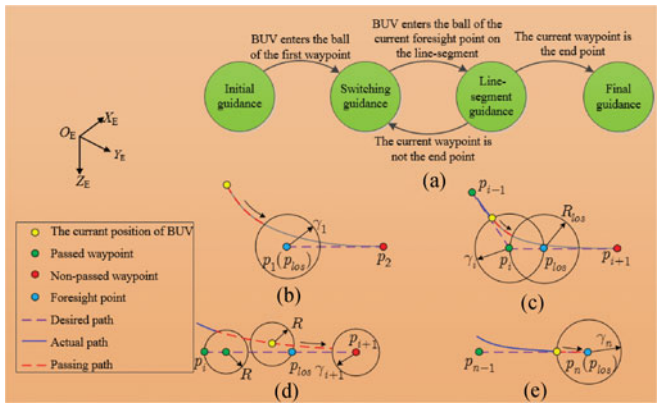

Fig. 8. LOS guidance system. (a) FSM. (b) Initial guidance. (c) Switching guidance. (d) Line-segment guidance. (e) Final guidance.

"RobCutt-I," as shown in Fig. 8, where $p_{\text{los}}(x_d, y_d, z_d)$ represents the foresight point of the LOS. Waypoint tracking is composed of initial guidance, switching guidance, line-segment guidance, and final guidance phases. Fig. 8(a) illustrates the robot's progress from the initial position into the ball of the first waypoint, which is called the initial guidance phase. The first waypoint serves as the foresight point of the LOS during this process. Once the BUV enters the ball of the first waypoint, the initial guidance ends and the switching guidance phase begins. Fig. 8(b) illustrates the switching guidance phase. Here, $L_{p_{i-1}p_i}$ represents the current tracking path, and $L_{p_i p_{i+1}}$ represents the next tracking path. The point on the line-segment $L_{p_i p_{i+1}}$ serves as the foresight point of the LOS during this process. The distance between this foresight point and p_i is γ_i. Once the BUV enters the p_{los} ball, the switching guidance ends and the line-segment guidance begins. Fig. 8(c) illustrates the process of line-segment guidance. The objective of this process is to reduce the distance error between the BUV and the desired path. The neighborhood ball of radius R, whose

center is the robot's current position, is denoted by $B_R(\text{BUV})$. If $B_R(\text{BUV})$ intersects line-segment $L_{p_i p_{i+1}}$ at two points, one of the two crossing points is selected as the LOS foresight point. The distance between this crossing point and p_{i+1} is shorter than the one between the other crossing point and p_{i+1}. If, instead, $B_R(\text{BUV})$ does not intersect line-segment $L_{p_i p_{i+1}}$ or intersects line-segment $L_{p_i p_{i+1}}$ only at one point, the point that is both on the current tracking line-segment and closest to the robot's current location is selected as the LOS foresight point. Note that the foresight point is related to the current position of the robot during this process. Namely, the foresight point changes along with the progress of the robot. Once the robot enters the ball of p_{i+1}, line-segment guidance ends. At this time, if p_{i+1} is the final point, final guidance begins. In this phase, the final waypoint is selected as the LOS foresight point. Otherwise, switching guidance begins again.

The desired course and depth are determined according to the LOS foresight point. The desired course is given as

$$\psi_d = \begin{cases} \pi + \frac{1}{2}\mathrm{g}(y_e)\cdot\pi & x_e = 0 \\ \arctan(\frac{y_e}{x_e}) + \pi + \frac{1}{2}\mathrm{g}(y_e)\cdot\pi - \\ \frac{1}{2}\mathrm{g}(x_e)\cdot\mathrm{g}(y_e)\cdot\pi & x_e \neq 0 \end{cases} \tag{8}$$

where $x_e = x_v - x_d$, $y_e = y_v - y_d$, $g(\ell) = \begin{cases} 1, & \ell \geq 0 \\ -1, & \ell < 0 \end{cases}$. The desired depth is selected as the depth of the foresight point.

C. Experimental Results

In order to verify the feasibility and effectiveness of waypoint tracking, a waypoint tracking experiment was conducted in the same swimming pool used in the other experiments. The desired path was a curve with a "⊃" shape. Six waypoints were chosen: p_1: $(1.5, 1.0, 0.2)$, p_2: $(3.0, 1.0, 0.3)$, p_3: $(4.0, 1.5, 0.4)$, p_4: $(4.0, 2.5, 0.4)$, p_5: $(3.0, 3.0, 0.2)$, p_6: $(1.5, 3.0, 0.1)$. The initial position of "RobCutt-I" (denoted as p_0) was $(1.147, 2.044, -0.032)$, and the initial yaw angle was 5.655 rad. Only the radius of the neighborhood ball of the final waypoint was 0.05 m. The radii of all the other waypoint balls were 0.2 m, Moreover, the radius of the neighborhood ball of "RobCutt-I" was 0.2 m as well. Fig. 9(a) shows the desired and actual paths of the BUV. Fig. 9(b) shows the time history of the cross-track error. Fig. 9(c) shows the time history of deflection angle of undulatory fins. Note that the deflection angles of the left and right long fins are always the same, and turning motion of the robot could be realized by regulating different wave frequencies of two long fins. Fig. 9(d) shows images of the waypoint tracking experiment. Note that the same scene was captured by two cameras (one is installed above the pool and another one is installed under the water surface) simultaneously. For the snapshots captured by underwater camera, the below image is the real image of "Robcutt-I" prototype and the top image is the reflective image. The reflective plane is the water surface, which is indicated by white line in Fig. 9(d).

The position of "RobCutt-I" is currently calculated and obtained by a sensor fusion of the global vision and water pressure sensor. This measurement is feasible in indoor environment. If

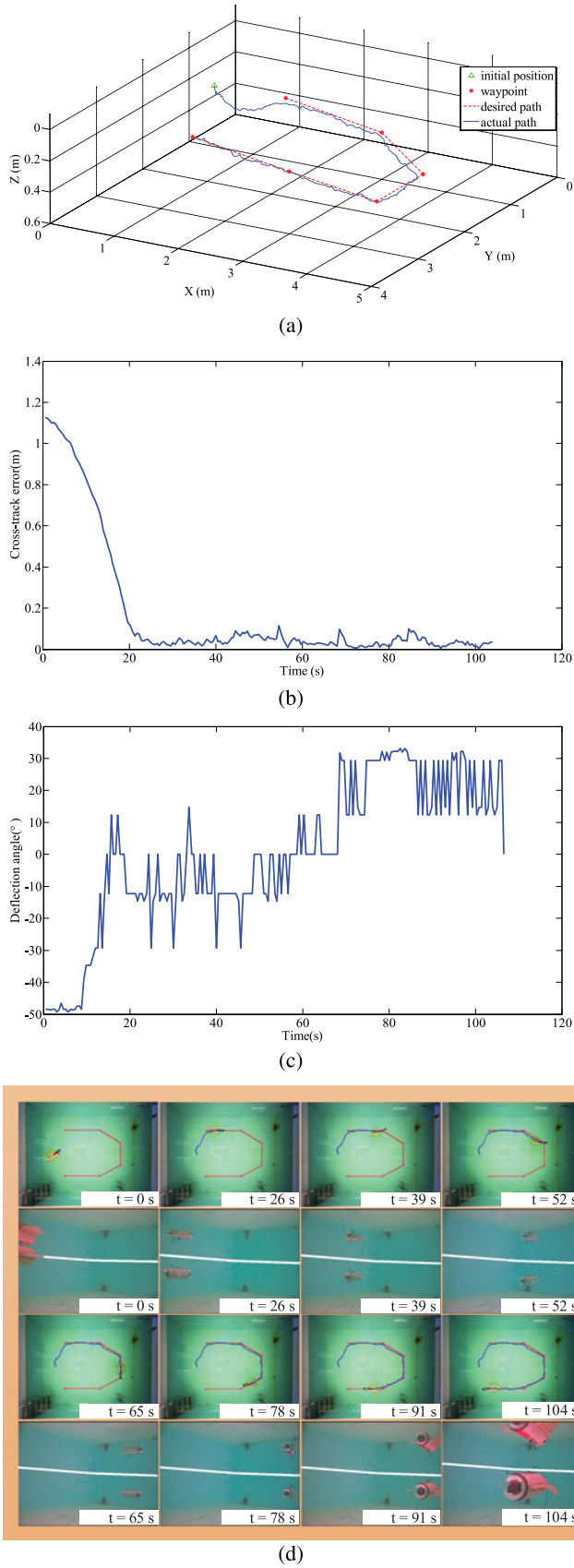

Fig. 9. Results of waypoint tracking. (a) Desired path and actual path in *x-y-z* space. (b) Cross-track error. (c) Deflection angles of undulatory fins. (d) Waypoint tracking images.

"RobCutt-I" is employed in a river or lake, an AHRS is used to measure its position and attitude. However, the proposed methods for depth/course control and waypoint tracking are still valuable.

Remark 1: The deflection angle of two long fins can be regulated to produce the pitch force along the whole body of the bio-inspired robot. Thus, its depth control can be realized by controlling fin surfaces.

VI. Conclusion and Future Work

In this paper, a bio-inspired robot with undulatory fins was constructed. The control methods for the swimming motions of this robot prototype were presented and described, comprising basic motion control, hybrid control for depth and course control, and waypoint tracking. The basic motion control reveals the relationship between average locomotion speed and kinematic parameters of the propagating waveform. A hybrid control consisting of an ADRC and a fuzzy method was used to achieve closed-loop depth and course control. Waypoint tracking was designed to help the bio-inspired robot with undulatory fins arrive at the assigned points to accomplish its tasks. Experimental results in an indoor swimming pool further showed the effectiveness of the proposed control methods.

Recently, the control methods of this prototype have only been verified in closed-water systems. The next generation of the bio-inspired robot with undulatory fins will be tested in a lake or a river. Future research will concentrate on two aspects: first, disturbance restrict and stable attitude control under natural uncertain disturbance will be explored; second, an underwater bio-inspired vehicle-manipulator system will be developed based on our previous work [26], and its autonomous operation will be studied.

References

[1] M. Sfakiotakis, D. M. Lane, and J. B. C. Davies, "Review of fish swimming modes for aquatic locomotion," *IEEE J. Ocean. Eng.*, vol. 24, no. 2, pp. 237–252, Apr. 1999.

[2] C. M. Breder, "The locomotion of fishes," *Zoologica*, vol. 4, no. 2, pp. 159–256, 1926.

[3] Z. Chen, S. Shatara, and X. Tan, "Modeling of biomimetic robotic fish propelled by an ionic polymerCmetal composite caudal fin," *IEEE/ASME Trans. Mechatronics*, vol. 15, no. 3, pp. 448–459, Jun. 2010.

[4] Y. J. Park, U. Jeong, J. Lee, S.-R. Kwon, H.-Y. Kim, and K.-J. Cho, "Kinematic condition for maximizing the thrust of a robotic fish using a compliant caudal fin," *IEEE Trans. Robot.*, vol. 28, no. 6, pp. 1216–1227, Dec. 2012.

[5] V. Kopman and M. Porfiri, "Design, modeling, and characterization of a miniature robotic fish for research and education in biomimetics and bioinspiration," *IEEE/ASME Trans. Mechatronics*, vol. 18, no. 2, pp. 471–483, Apr. 2013.

[6] Z. Su, J. Yu, M. Tan, and J. Zhang, "Implementing flexible and fast turning maneuvers of a multijoint robotic fish," *IEEE/ASME Trans. Mechatron.*, vol. 19, no. 1, pp. 329–338, Feb. 2014.

[7] C. Zhou and K. H. Low, "Design and locomotion control of a biomimetic underwater vehicle with fin propulsion," *IEEE/ASME Trans. Mechatron.*, vol. 17, no. 1, pp. 25–35, Feb. 2012.

[8] Y. Wang, J. Tan, and D. Zhao, "Design and experiment on a biomimetic robotic fish inspired by Freshwater Stingray," *J. Bionic Eng.*, vol. 12, no. 2, pp. 204–216, 2015.

[9] B. Allotta, "The ARROWS project: Adapting and developing robotics technologies for underwater archaeology," in *Proc. 4th IFAC Workshop Navig., Guid. Control Underw. Veh.*, Girona, Spain, 2015, pp. 194–199.

[10] C. Georgiades, A. German, A. Hogue, and W. Daviddi, "AQUA: An aquatic walking robot," in *Proc. IEEE/RSJ Int. Conf. Intell. Robots Syst.*, Sendai, Japan, 2004, pp. 5015–5020.

[11] G. Dudek, "A visually guided swimming robot," in *Proc. IEEE/RSJ Int. Conf. Intell. Robots Syst.*, Edmonton, AB, Canada, 2005, pp. 3604–3609.

[12] O. M. Curet, A. N. Patankar, G. V. Lauder, and M. A. MacIver, "Mechanical properties of a bio-inspired robotic knifefish with an undulatory propulsor," *Bioinspirat. Biomimet.*, vol. 6, no. 2, p. 026004, 2011.

[13] F. Liu, K. M. Lee, and C. J. Yang, "Hydrodynamics of an undulating fin for a wave-like locomotion system design," *IEEE/ASME Trans. Mechatron.*, vol. 17, no. 3, pp. 554–562, Jun. 2012.

[14] K. H. Low, "Modelling and parametric study of modular undulating fin rays for fish robots," *Mech. Mach. Theory*, vol. 44, pp. 615–632, 2009.

[15] C. Zhou and K. H. Low, "On-line optimization of biomimetic undulatory swimming by an experiment-based approach," *J. Bionic Eng.*, vol. 44, pp. 213–225, 2014.

[16] Y. Zhang, J. He, and K. H. Low, "Parametric study of an underwater finned propulsor inspired by bluespotted ray," *J. Bionic Eng.*, vol. 9, no. 2, pp. 166–176, 2012.

[17] G. Wang, X. Ma, T. Hu, and D. Zhang,"Experimental and analytical study on factors influencing biomimetic undulating fin propulsion performance based on orthogonal experimental design," *Adv. Robot.*, vol. 27, no. 8, pp. 597–609, 2013.

[18] T. Hu, K. H. Low, L. Shen, and X. Xu, "Effective phase tracking for bioinspired undulations of robotic fish models: A learning control approach," *IEEE/ASME Trans. Mechatronics*, vol. 19, no. 1, pp. 191–200, Feb. 2014.

[19] M. M. Rahman, S. Sugimori, H. Miki, R. Yamamoto, Y. Sanada, and Y. Toda, "Braking performance of a biomimetic squid-like underwater robot," *J. Bionic Eng.*, vol. 10, no. 3, pp. 265–273, 2013.

[20] L. Shang, S. Wang, M. Tan, and L. Cheng, "Swimming locomotion modeling for biomimetic underwater vehicle with two undulating long-fins," *Robotica*, vol. 30, no. 6, pp. 913–923, 2012.

[21] Q. Wei, S. Wang, X. Dong, L. Shang, and M. Tan, "Design and kinetic analysis of a biomimetic underwater vehicle with two undulating long-fins," *Acta Autom. Sinica*, vol. 39, no. 8, pp. 1330–1338, 2013.

[22] F. Giorgio-Serchi, F. Renda, M. Calisti, and C. Laschi, "Thrust depletion at high pulsation frequencies in underactuated, soft-bodied, pulsed-jet vehicles," in *Proc. MTS/IEEE OCEANS Conf.*, Genoa, Italy, 2015, pp. 1–6.

[23] J. Han, "From PID to active disturbance rejection control," *IEEE Trans. Ind. Electron.*, vol. 56, no. 3, pp. 900–906, Mar. 2009.

[24] M. Sfakiotakis, J. Fasoulas, and R. Gliva, "Dynamic modeling and experimental analysis of a two-ray undulatory fin robot," in *Proc. IEEE/RSJ Int. Conf. Intell. Robots Syst.*, Hamburg, Germany, 2015, pp. 339–346.

[25] T. I. Fossen, *Marine Control Systems: Guidance, Navigation and Control of Ships, Rigs and Underwater Vehicles* Tiller, Norway: Marine Cybernetics, 2002.

[26] Y. Wang, S. Wang, Q. Wei, M. Tan, C. Zhou, and J. Yu, "Development of an underwater manipulator and its free-floating autonomous operation," *IEEE/ASME Trans. Mechatron.*, vol. 21, no. 2, pp. 815–824, Apr. 2016.

Shuo Wang received the B.E. degree in electrical engineering from the Shenyang Architecture and Civil Engineering Institute, Shenyang, China, the M.E. degree in industrial automation from the Northeastern University, Shenyang, and the Ph.D. degree in control theory and control engineering from the Institute of Automation, Chinese Academy of Sciences, Beijing, China, in 1995, 1998 and 2001, respectively.

He is currently a Professor in the State Key Laboratory of Management and Control for Complex Systems, Institute of Automation, Chinese Academy of Sciences. His research interests include biomimetic robot, underwater robot, and multirobot systems.

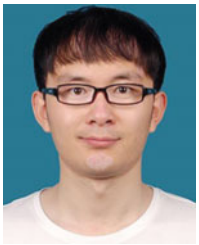

Yu Wang received the B.E. degree in automation from Beijing Institute of Technology, Beijing, China, and the Ph.D. degree in control theory and control engineering from Institute of Automation, Chinese Academy of Sciences, Beijing, in 2011, 2016, respectively.

He is currently an Assistant Professor in the State Key Laboratory of Management and Control for Complex Systems, Institute of Automation, Chinese Academy of Sciences. His research interests include intelligent control, robotics, and biomimetic robots.

Qingping Wei received the B.E. degree in automation from University of Electronic Science and Technology of China, Chengdu, China, in July 2010, and the Ph.D. degree in control theory and control engineering from the State Key Laboratory of Management and Control for Complex Systems, Institute of Automation, Chinese Academy of Sciences, Beijing, China, in July 2015.

He is currently a Researcher for Dongfang Electric Corporation. His research interests include intelligent control and robotics.

Min Tan received the B.E. degree in control engineering from Tsinghua University, Beijing, China, and the Ph.D. degree in control theory and control engineering from the Institute of Automation, Chinese Academy of Sciences, Beijing, in 1986 and 1990, respectively.

He is currently a Professor in the State Key Laboratory of Management and Control for Complex Systems, Institute of Automation, Chinese Academy of Sciences. His research interests include advanced robot control, biomimetic robot, multirobot system.

Junzhi Yu (SM'14) received the B.E. degree in safety engineering and the M.E. degree in precision instruments and mechanology from the North China Institute of Technology, Taiyuan, China, in 1998 and 2001, respectively, and the Ph.D. degree in control theory and control engineering from the Institute of Automation, Chinese Academy of Sciences, Beijing, China, in 2003.

He is currently a Professor with the State Key Laboratory of Management and Control for Complex Systems. His research interests include biomimetic robots, intelligent control, and intelligent mechatonic systems.

Dr. Yu serves as the Associate Editor of the IEEE TRANSACTIONS ON ROBOTICS and *Journal of Mechanical Science and Technology*, and as the Technical Editor of the IEEE/ASME TRANSACTIONS ON MECHATRONICS.